Received: October 12, 2024. Revised: January 3, 2025. 160

International Journal of
Intelligent Engineering & Systems

http://www.inass.org/

Optimized Bisection Image Processing for Wave Identification in Two-Phase Flow on Narrow Gap Rectangular Channel

Nur Rahmad Yusuf[1,2] Suprapto[2]* Jazi Eko Istiyanto[2] Deendarlianto[3]

[1]*Directorate of Inspection for Nuclear Installation and Material BAPETEN, Jl. Gajah Mada 8, Jakarta, Indonesia*
[2]*Department of Computer Science and Electronics Universitas Gadjah Mada, Bulaksumur, Yogyakarta, Indonesia*
[3]*Department of Mechanical and Industrial Engineering Universitas Gadjah Mada, Bulaksumur, Yogyakarta, Indonesia*
*Corresponding author's Email: sprapto@ugm.ac.id

Abstract: Accurate wave identification in two-phase flows is critical for assessing cooling processes in narrow rectangular channels, especially in post-accident scenarios such as those at Three Mile Island and Fukushima. This study introduces a novel image processing technique that enhances wave identification through a sequential thresholding and image bisection methods. Unlike conventional methods, this method iteratively adjusts thresholds, optimizing image segmentation for low-quality images in real-time applications. Examination on 3000 jpeg images in the resolution 592 x 192 show that proposed method has significant improvement. The proposed approach achieves significant improvements in wave identification accuracy, with RMSE reductions ranging from 75.45% to 94.50%, enabling more precise measurements of film thickness and wave interface behavior. These advancements support enhanced real-time monitoring for nuclear reactor cooling systems, offering substantial contributions to safety protocols during critical events.

Keywords: Image optimization, Multi-threshold, Rectangular channel, Two-phase flows, Raw image, Wave identification, Bisection methods, Nuclear reactor cooling.

1. Introduction

The phenomenon of gas-liquid stratification and wavy flow is critical in many engineering applications, especially in ensuring the safety of nuclear power plants with light water reactors. Incidents like the Three Mile Island (1979) and Fukushima Daiichi (2011) accidents have highlighted the importance of managing thermal hydraulics to maintain reactor pressure vessel (RPV) integrity during loss-of-coolant accidents (LOCA) [1, 2]. In such events, damage to the RPV raises concerns about leakage, emphasizing the need for reliable cooling in the narrow gaps between debris and the RPV wall [3, 4].

Two-phase flows, where interfacial waves arise due to gas-liquid velocity differences, affect key flow characteristics such as pressure drop and heat transfer rates [5, 6]. Therefore, accurately detecting and analyzing these waves is crucial to preventing reactor malfunctions. However, existing wave identification methods face significant challenges in narrow-gap channels.

Conventional methods, such as conductance probes and capacitance probes, provide valuable measurements but are intrusive, potentially altering the flow dynamics under investigation [7-12]. Additionally, while high-speed videometry offers non-intrusive identification, it requires substantial computational power, making it less feasible for real-time applications in nuclear reactors, where rapid, accurate monitoring is essential for safety [13]. These limitations hinder the effective identification of wave patterns in critical flow environments, especially in situations involving low-quality images and narrow spaces.

Image processing has emerged as a non-intrusive alternative, allowing real-time analysis of wave patterns in two-phase flows. This approach offers advantages such as easy calibration and adaptability across different flow regimes. However, current image processing methods often struggle with low-quality images, which suffer from poor lighting, low resolution, or low contrast, impacting wave identification accuracy [13-17].

This study introduces a novel image processing method specifically designed to overcome the challenges of wave identification in two-phase flows. The method employs sequential image optimization, enhancing raw image quality through advanced morphological operations that improve contrast, resolution, and geometric accuracy. This approach enables precise identification of wave dynamics, even from low-quality input images, while remaining non-intrusive and computationally efficient—making it ideal for real-time monitoring in narrow-gap channels. Such capability is critical for ensuring nuclear reactor safety during LOCA events. By addressing persistent issues like poor image quality and the constraints of narrow geometries, the proposed method establishes itself as a strong point in wave identification and image processing, offering a robust, scalable, and highly accurate solution that outperforms conventional techniques.

The remainder of this paper is organized as follows: Section 2 reviews modern techniques for liquid film thickness identification. Section 3 explains the image optimization process, and Section 4 details the operational framework of the proposed method. Section 5 summarizes the contributions and suggests future research directions.

2. Related work

Accurate wave identification and liquid film thickness measurement are crucial for optimizing the performance and ensuring the safety of gas-liquid two-phase flow systems. These systems are foundational in industries such as nuclear reactor cooling, chemical processing, and oil and gas transportation, where precise control of fluid dynamics is essential for maintaining operational stability and efficiency. However, traditional intrusive techniques, such as conductance and capacitance probes, often disrupt the flow dynamics, leading to potential inaccuracies. These methods are particularly limited in narrow or complex geometries, where their applicability becomes constrained. Consequently, the demand for non-intrusive, real-time image processing techniques that offer high-accuracy measurements under challenging conditions, without altering the natural flow, has grown significantly.

Intrusive methods, as observed by Mantilla et al. [18], introduce disturbances that compromise the accuracy of flow monitoring, particularly in critical systems like nuclear reactors. To mitigate these issues, researchers have turned to non-intrusive methods such as high-speed videometry, which has demonstrated potential for capturing dynamic behaviors in two-phase flows. As described in [19], for example, showed that high-speed videometry could effectively monitor bubble-to-slug transitions, achieving significant improvements in measurement precision. However, such techniques are often hampered by limitations in lighting, resolution, and computational efficiency, which diminish their reliability in industrial settings. These challenges necessitate advanced methodologies capable of addressing these drawbacks while maintaining robust performance in dynamic and noisy conditions.

The research survey in Table 1 highlights key limitations in existing wave identification techniques. Methods such as wavelet-based approaches, while effective, impose high computational demands that restrict their scalability for real-time applications. Moreover, the reliance on high-quality input images presents a significant barrier in industrial environments, where imaging conditions are frequently suboptimal due to poor lighting or noise. The lack of adaptability to narrow or geometrically complex environments further constrains their applicability in critical systems like nuclear reactors and chemical processing plants.

The complexity of image processing methods is a critical factor in determining their performance and applicability. Table 1 categorizes methods into Low, Moderate, and High complexity based on computational demands, preprocessing steps, and adaptability to varying conditions. Low complexity methods, such as those used in [20], rely on basic techniques like grayscale conversion [21] and thresholding[22]. While computationally efficient, these methods often fail to handle complex flow dynamics, especially in industrial environments with varying lighting or noise. Moderate complexity methods, like those employed in [23], balance accuracy and computational effort by incorporating techniques such as noise reduction and edge identification. However, the increased computational load can hinder their applicability in real-time scenarios.

High complexity methods, such as those used in [24] and in the current study, employ advanced techniques like multi-thresholding and adaptive

Table 1. Comprehensive review of image processing techniques for wave identification and liquid film thickness measurement in gas-liquid two-phase flow systems

Author, (Year)	Geometry and orientation	The working of fluid	Enhancement methods	Data set	Complexity	Drawbacks
Deendarlianto, et al.[26] (2019)	Position Pipe horizontal, Diameter 26 mm	Water - Air	• High-speed camera-visualization • Image processing for Liquid film thickness and wave parameter	Video image 1280 × 800 pixels; 400–1200 fps	Moderate	High dependence on image quality; limited validation metrics
Wijayanta et al [23], (2022)	Horizontal Pipe Section: Diameter: 25.4 mm (approximately 1 inch), Length: 635 mm. Inclined Inclination Angle: 50°.	Water: Mixed with 40% glycerol, Air	• Grayscale Conversion, • Background Subtraction, • Noise Reduction, • Contrast Enhancement, • Binary Conversion • Thresholding, • Edge Detection, • Smoothing and Contour Refinement, • Geometric Calibration • Measurement Unit conversion	Video image 120-240 fps	Moderate	Limited adaptability to narrow geometries; computational overhead.
Wijayanta et al [27], (2023)	horizontal acrylic pipe with an inner diameter of 26 mm and a length of 9500 mm.	various liquids (e.g., water, glycerol-water mixtures, Air	• Noise Reduction (Median Filtering), • Image Complement, • Background Subtraction, • Contrast Enhancement, • Smoothing	Video image 120-240 fps	High	Computationally intensive; scalability issues in real-time applications
Nugroho et al, [24], (2024)	horizontal and inclined pipe connected by an elbow	Air, water	• Grayscale Conversion, • Background Subtraction, • Noise Reduction, • Contrast Enhancement, • Binary Conversion, • Smoothing, and • Contour Refinement	Video image; 240 fps	High	High computational demand; unsuitable for real-time applications.
Astyanto et al, [20], (2023)	Horizontal Pipe Section: Diameter: 25.4 mm (1 inch), Angle of Inclination: Typically set between 10° to 20° relative to the horizontal plane	40% glycerol-water mixture, Air,	• Grayscale Conversion, • Background Subtraction, • Noise Reduction, • Contrast Enhancement, • Binary Conversion and Thresholding, • Edge Detection, • Smoothing and Contour Refinement, • Geometric Calibration • Measurement Unit Conversion	Video image; 240 fps	Low	Simplistic methods; poor performance in handling complex flow dynamics
Current study	Position Vertical rectangular channel Width 50, length 1100 mm and depth 4mm	saturated water-steam	• Sequential Thresholding: • Binary Conversion • Morphological Operations: • Brightness Adjustment • Multi-Selection Thresholding	Image 592 × 192 pixels; 1000 fps	High	Requires preprocessing resources but offers high adaptability and precision

morphological operations [25]. These methods excel in providing high accuracy and adaptability, making them well-suited for challenging industrial conditions. The trade-off, however, is their significant computational demand, which can limit real-time applicability. The proposed method addresses this limitation by employing techniques that balance accuracy and computational efficiency, such as sequential thresholding and brightness adjustments. This ensures robust performance under

real-time industrial conditions while maintaining adaptability to diverse geometries and suboptimal imaging environments.

To overcome the limitations identified in Table 1, the proposed method introduces advanced image processing techniques that leverage multi-thresholding to dynamically adjust segmentation thresholds based on regional image characteristics. This approach ensures robust segmentation in environments with varying lighting or noise, surpassing the limitations of basic thresholding techniques like those employed in [20].

Furthermore, by integrating sequential thresholding and adaptive morphological operations, the method significantly reduces computational demands, enabling real-time scalability. Unlike previous studies in [24], which relied on lower temporal resolutions (240 fps), the current study employs datasets with a higher frame rate (1000 fps), ensuring greater accuracy in capturing rapid wave dynamics.

The proposed method's focus on narrow rectangular channels addresses the geometric limitations identified in earlier works. While studies such as [23] investigated inclined and horizontal configurations, they demonstrated limited adaptability to confined spaces. The proposed method bridges this gap, enhancing its suitability for industrial systems with narrow-gap geometries.

The insights gained from the research survey also guided the selection of meaningful benchmarks for comparison. Computationally intensive techniques like wavelet-based methods [24] and methods reliant on high-quality imagery [26] were identified as critical reference points. The proposed method addresses the shortcomings of these techniques by offering quantitative validation and superior performance under challenging conditions. Moreover, the detailed dataset specifications in this study resolve common gaps in earlier research, enabling fair and comprehensive evaluations against existing methodologies.

The proposed method's effectiveness is demonstrated through measurable improvements in segmentation accuracy, computational efficiency, and adaptability. Its ability to operate in narrow geometries and under diverse flow conditions makes it particularly suitable for critical applications, such as nuclear reactor cooling and chemical processing. By addressing long-standing challenges, the method provides a robust and scalable solution that advances the field of wave identification and liquid film thickness measurement. These findings establish a foundation for further exploration into real-time monitoring, system optimization, and broader industrial applications.

The progression from traditional intrusive techniques to advanced non-intrusive image processing marks a transformative advancement in the analysis of gas-liquid two-phase flows. While significant progress has addressed disruptive measurement methods and scalability challenges, persistent issues—such as high computational demands, limited adaptability to narrow geometries, and reliance on high-quality input images—underscore the need for innovative solutions tailored to complex industrial environments.

By addressing these specific gaps, as highlighted in Table 1, the proposed method integrates advanced image processing techniques that achieve substantial improvements in segmentation accuracy, computational efficiency, and adaptability. Its capability to perform under diverse and challenging conditions, including narrow-gap configurations and suboptimal imaging environments, reinforces its industrial relevance and scalability. Moreover, the study's focus on transparency and reproducibility, through detailed dataset specifications and meaningful benchmarks, strengthens its contribution to advancing wave identification and liquid film thickness measurement techniques.

This section has outlined the limitations of existing methodologies, the insights gained from prior research, and the advancements achieved through the proposed approach. By bridging these gaps, the proposed method lays a strong foundation for real-time monitoring, system optimization, and broader applications in complex industrial systems. The next section delves into the technical framework and methods that underpin these advancements, providing a detailed explanation of the methodologies that drive this transformative approach.

3. Material and method

The experimental setup, involved the HeaTiNG-02 (Heat Transfer in Narrow Gap-02) test section, simulating the debris and cooling processes of the Reactor Pressure Vessel (RPV) following the TMI-2

accident. The setup consisted of two SS316 stainless steel heated plates (8 mm thick, 50 mm wide, 1000 mm long) and a 4 mm thick heated plate, with a 2 mm quartz glass panel used for enhanced visibility. The channel measured 50 mm in diameter, 1100 mm in length, and had a width-to-gap aspect ratio of 12.5.

The experiment was conducted under atmospheric pressure, assuming no heat transfer across the system boundary. Halogen bulbs were used to illuminate the flow patterns, while high-speed video cameras captured the boiling flow during quenching at 1000 frames per second with a resolution of 800x600 pixels. The substrate was heated by open coil ceramic heaters until the plate reached 1000°C, after which water was introduced into the channel at a flow rate of 0.089 kg/s with an average temperature of 98°C. The experiment was halted when the plate cooled to 100°C.

A 3-second video was captured, resulting in 3000 JPEG images at a resolution of 592x192 pixels. These images were processed using Python 3.12.0 and the OpenCV library, on a system equipped with an Intel® Core™ i7-10750H @ 2.60 GHz processor, 64 GB DDR4 RAM, and a 4 GB GDDR6 GPU, running on Windows 11. Full details of the experimental equipment and procedures can be found in previous publications [4, 28-30].

4. Proposed method

Raw image quality is crucial in image processing, as it directly influences the accuracy and reliability of liquid film thickness measurements. Image enhancement is a vital technique in this domain, aimed at improving image quality for specific applications such as analysis, identification, segmentation, and recognition [31]. For these processes to be effective, the image must possess balanced technical qualities, including appropriate sharpness, exposure, noise levels, and color accuracy. These aspects are essential to ensure that the image is both visually clear and informative [32]. Through enhancement, an image can achieve the quality necessary to provide accurate data, which is critical for subsequent analysis and processing.

Creating a system that effectively improves images universally is a complex undertaking. The use of unenhanced image enhancement methods, the choice of assessment index, noise impact and selection of optimum parameters are major factors that contribute to this issue [33].

The process of determining the level of accuracy is known as image quality assessment (IQA). In order to assess the quality of an image, two methods may be applied: subjective and objective. Subjective approaches rely on a human observer's subjective assessment of an image or a collection of images' characteristics. On the other hand, objective methods are grounded in computational models that can anticipate the perceptual quality of an image. In this study, the evaluation of image quality is conducted using both subjective and objective measures [33].

A comprehensive overview of the optimization of image processing techniques will be presented in this section.

The experimental works used in this research highly relied on image processing techniques comprising two main stages: frame pre-processing and water surface level measurement. The pre-processing stage itself consists of several steps. The successive processes of image processing employed in the current study are illustrated in Fig. 2. After documenting the two-phase flow phenomenon, it was uploaded to a personal computer (PC) using the AOS Technologies AG Imaging Studio program. The recorded video has three color channels: RGB (red, green, and blue).

The 3-channel raw images were subsequently edited to remove superfluous areas. The scholarly articles written by [16] and [17] provide comprehensive insights into image processing techniques. Although the camera placement has been carefully calibrated in this experiment, there is still a misalignment of the horizontal axis of the channel and the image that requires rotation.

The video files were converted into grayscale image frames and imported into Python for analysis. As detailed in the Materials and Methods section, the dataset consists of 3000 JPEG images extracted from a 3-second video with a resolution of 592x192 pixels, captured at 1000 frames per second. This dataset was processed using Python 3.12.0 and the OpenCV library within Visual Studio Code (v1.83.1), utilizing the hardware configuration previously described. Pre-processing and analysis were applied to the dataset to optimize the identification and measurement of liquid film thickness.

The image frames are loaded sequentially according to their order. From a technical standpoint, the loaded frame is then transformed into grayscale. This particular scenario does not require all color channels for analysis. This particular analysis scenario does not always require retaining all color channels. The single-color channel image will be divided into several parts along the horizontal axis.

Each part will be subjected to color thresholding with different threshold values.

The purpose of such a division process is to introduce flexibility in analyzing each image part regarding the threshold value The objective of

thresholding itself is to obtain a binary image in this particular case, the region filled with water will be colored black, while the area filled with air will be converted to white.

The region is made up of the fact that, as seen in the original image, the water area seems to be darker than the atmosphere.

However, the resulting image of this process might not look as clear as expected, thanks to the appearance of noise. A morphological closing operation addressed this issue and eliminated small black regions in the white segment. The entire pre-processing process can be seen in Fig. 1.

As the pre-processing has been completed, the next thing to be done is to measure the film thickness. We created reference points near the image based on the horizontal axis to measure the film thickness.

There were 28 reference points employed in the experiment. We will iterate upwards for each point until a black pixel is found, indicating the air-water interface. In order to find the film thickness, the number of pixels was measured during iterations. The film thickness can be measured in millimeters when taking into account the actual channel dimension. The pseudocode of this process can be seen in the algorithm 1-surface point measurement.

Compared to another method flow diagram that utilizes image processing to detect and measure liquid film thickness, our proposed method aims to optimize the image processing method to process images of insufficient quality effectively to detect and measure liquid film thickness. That method can be observed in the accompanying Fig.2.

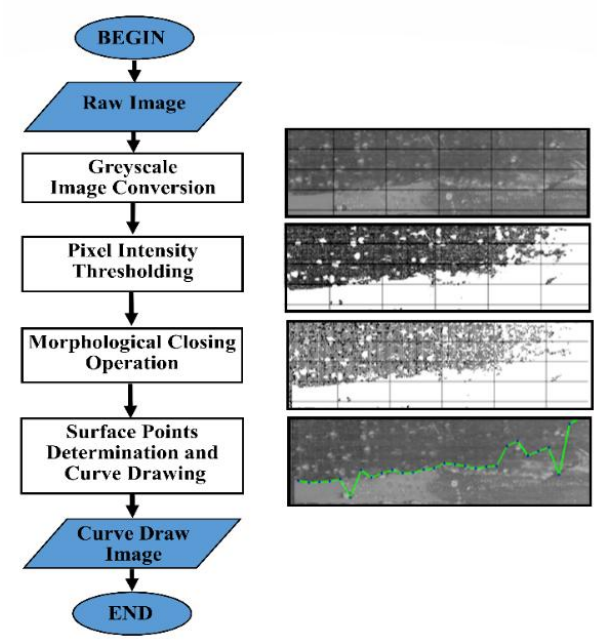

Figure. 1 The diagram of Pre-processing Steps and the right-side Corresponding Result

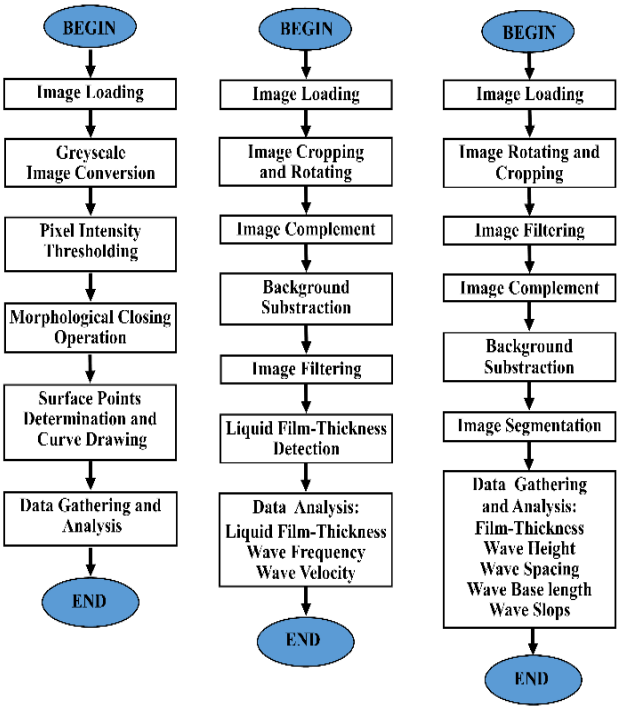

Figure. 2 (a) The proposed method, (b) Wijayanta et al [27] and (c) the method of Hudaya et al.[34]

The pre-processing phase in this study is simple compared to the pre-processing steps described in the earlier works of [26, 34] in Fig. 2 (b) and Fig 2 (c).

In the preceding method, the image was cropped and rotated before loading the image into the Python code. We use different approaches to improve the image quality for tasks such as image complement, image filtering, and background subtraction. This entails the conversion of the image to grayscale, the application of an intensity thresholding algorithm for pixels, and the performance of morphologic closing operations.

In contrast to [27], to improve image contrast and complement, the suggested method uses a morphological methodology that combines open and close operations. A single-level threshold is used for picture segmentation and background subtraction, and a median filter is also applied to minimize noise efficiently [27].

On the other hand, for these tasks, our study applies the closure morphological technique with a multi-selection threshold. In contrast to [27], the improvement process uses a morphological process (a mix of open and close), a bottom hat and top hat filter for image contrast, image complement, a median filter for noise removal, background removal, and image segmentation with a single-level threshold. This work, on the other hand, uses a multi-selection threshold and the closing morphological method.

This procedure enhances an image's overall visual fidelity before using Python programming. The optimization method in this image processing task entails the refinement of the threshold and segmentation of the image into two distinct regions. Each region can be individually changed to varying threshold values to attain the highest possible image quality. This process aims to improve the accuracy of identifying the interface between air and water.

Algorithm 1: Surface Point Mcasurement

Input: image[,]
Output: *point_height*
Data: *i,j*
/* $i \in \{0,1,2,\dots,width\}, j \in \{0,1,2,\dots,height\}$ */
for *each i* **do**
    point_height[i]
for *each i* **do**
    for *each j* **do**
        if *image[i,j]*=255 **then**
            $point\_height[i] \leftarrow point\_height[i] + 1$
        else
            Break

$Image[i,j]$ represent the pixel value at coordinates (i,j), where i ranges from 0 to $width-1$ and j ranges from 0 to $height-1$. The goal is to compute *point_height* [*i*] for each column *i*, which is defined as the number of white pixels (255) in that column.

The mathematical formulation algorithm and the pseudocode can be expressed as:

$$point\_height[i] = \sum_{j=0}^{height} [image\ [i,j] = 255] \quad (1)$$

where:

$$[P] = \begin{bmatrix} 1 & if\ P \text{ is } true \\ 0 & other \end{bmatrix}$$

$$point\_height\ [i] = 0,$$

$$point\_height[i] = 0, \forall\ i \in \{0,1,2,3\dots,width\}$$

In the proposed methodology, the indicator function [image[*i,j*]] plays a crucial role in identifying the presence of specific pixel values within the image matrix. Specifically, it returns a value of 1 if the pixel at position (*i, j*) holds the intensity value of 255, which is typically used to denote a particular feature or object of interest within the image. Conversely, it returns 0 for any other pixel value. The summation over the index j is then applied across each column i, effectively counting the total number of pixels with the intensity value of 255 within that column. This summation yields a column-wise result, denoted as $point\_height$ [*i*], which represents the cumulative height of the feature across each column. This process is independently executed for each column in the image, leading to the creation of the $point\_height$ array, where each entry corresponds to the height of surface points along the respective columns of the image.

5. Experiment and result

The presence of visual images of substandard quality presents difficulties for human perception as well as for applications in image processing and computer vision. Hence, enhancing the quality of images before their utilization is imperative to ensure their alignment with human visual perception, facilitate machine analysis, and improve the efficacy of computer vision applications.

While there are currently no set criteria for identifying optimum illumination and contrast levels, it is generally noted that images in non-standard lighting situations tend to demonstrate inferior quality. The conclusions published in past research, low contrast and inadequate lighting have constantly created significant obstacles in image processing, computer vision, and related domains. Lowlight images exhibit lower luminance and an uneven distribution of illumination, generally captured in situations with limited lighting circumstances [35].

The human eye can selectively process the impact of light and extract the surface reflectance of an object, enabling the perception of color [36]. Human visual perception possesses the ability to effectively assess the quality of images and detect disparities between images of low quality.

In order to determine the optimum brightness and threshold values for an image, a methodology suggested in this study shall be used, which facilitates optimization. The image will undergo sequential processing, with each stage analyzing-only three frames to get the optimal value. The image frame will utilize frame numbers 1000, 2000, and 3000.

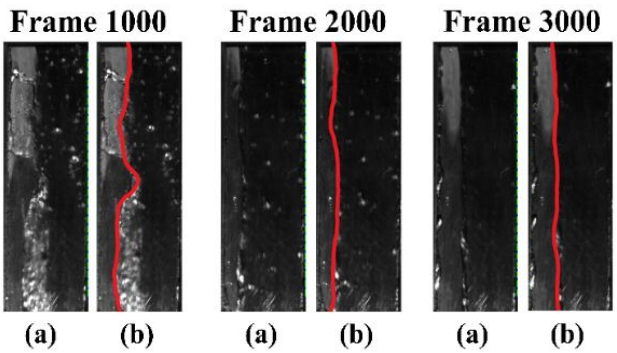

Figure. 3: (a) The three sample of pairs of Raw image and (b) Ground truth images

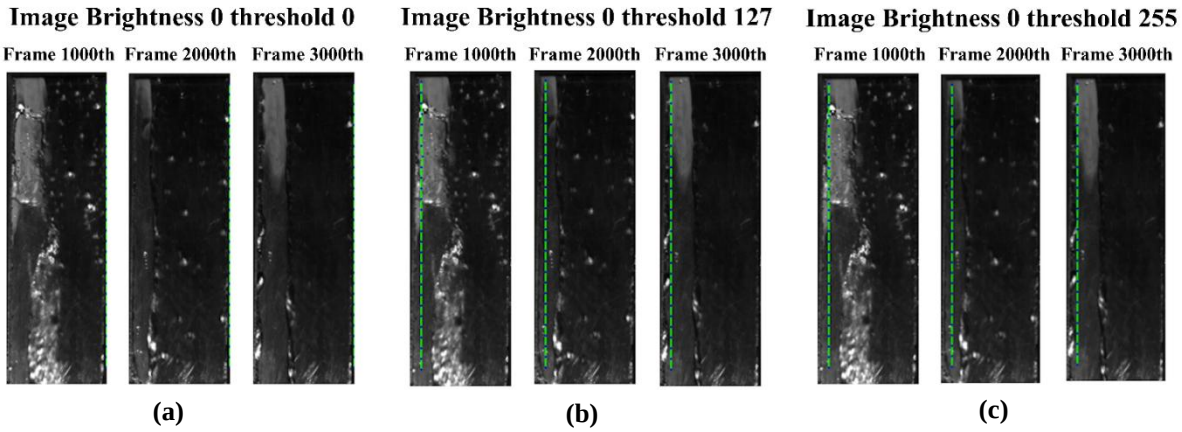

Figure. 4 Images for brightness of 0 and: (a) threshold=0, (b) threshold=127, and (c) threshold=255

Frame 1000th

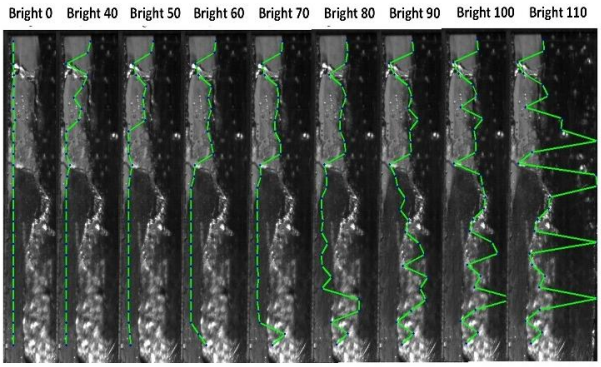

Figure. 5 Image on frame 1000th for threshold of 127 and brightness 0 up to 110

Frame 1000th Brightness

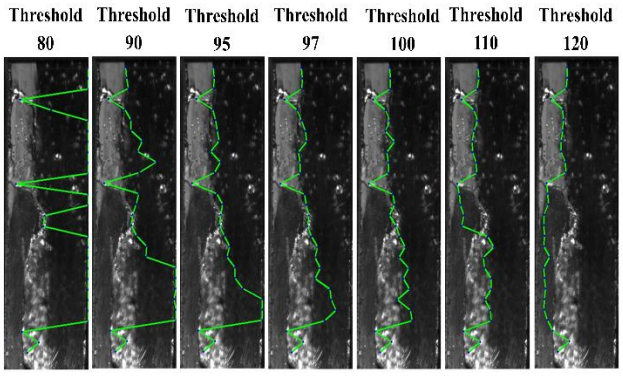

Figure. 6 Image on frame 1000th for the brightness of 70 and threshold of 80 up to 120

To evaluate the optimization outcomes, it is essential to have a foundational image that is a benchmark for comparing the initial image and the optimized results [37, 38]. This reference image, which remains unaltered by optimization techniques, is utilized to ascertain the perfect image for comparison purposes. The subsequent procedure involves determining the ideal value for brightness, which serves as the threshold for assessing image quality. The comparison of images possessing optimal values with reference images is conducted to evaluate image quality. This assessment relies on reference lines created by image processing and subsequent image comparison.

A) Reference images

The reference image in Fig. 3 is needed as a base image that will be used as a comparison image. The reference image in frames 1000th, 2000th, and 3000th will be divided into two types. The raw image (first image in a pair) and ground truth images (second image in a pair). The raw image means the raw image that has been processed in image processing without tuning in brightness or threshold values. In comparison, the ground truth image is one with a manually drawn line reference on the water interface, which is why this image is used as a standard image for comparison.

B) Optimization of brightness value and threshold

The next step is finding the optimal value of the threshold values 0, 127, and 255 without setting the brightest value. The next step will use this value as the base threshold value. Based on the raw image processed with the proposed method for frames 1000th, 2000th, and 3000th, only the image using threshold value 0 cannot detect the water surface Fig.4 (a), and the green line marks the water surface. The best threshold setting generates a green line mark ranging from 127 to 255. The resulting image highlights Fig. 5 (b) and (c) with a green line, as seen in Fig. 5. The threshold value of 127 is positioned at

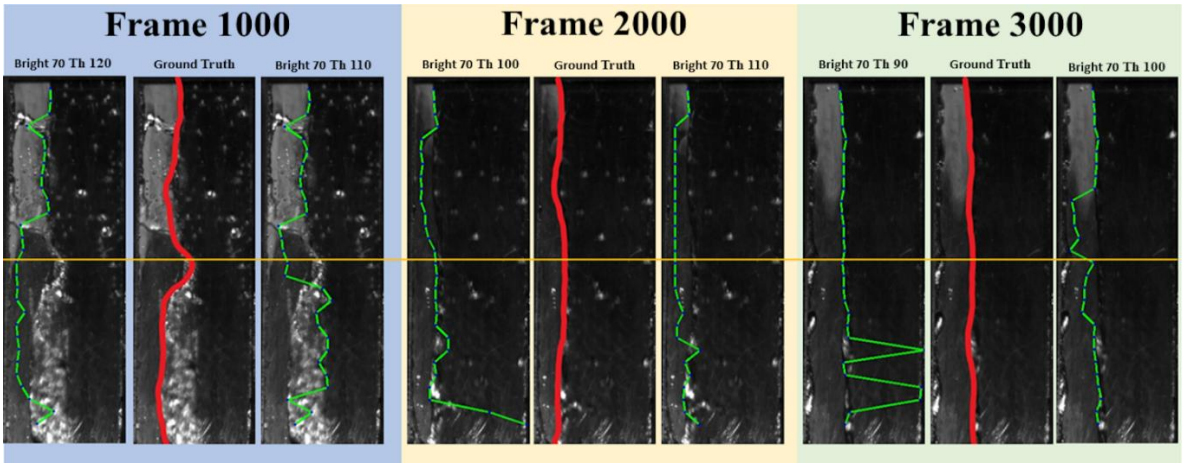

Figure. 7 Candidate image for frame 1000th, 2000th, and 3000th with various threshold

the midpoint of the threshold range, which spans from 0 to 255. This placement allows for greater flexibility in adjusting the threshold value in the subsequent phase.

In the next step, find the optimal brightness using a threshold value between 0 and 110 in Fig. 5, the processing image for frame 1000th. Using human observation, we choose the candidate with the best green line to fit the water and air interface. The best fit is at a brightness value of 70. For frames 2000th and 3000th, we use the same operation and choose the optimum brightness value for the next step

From the image processing observation of frames 1000th, 2000th, and 3000th, the optimum brightness value is 70. This value will be used for the next step to find the optimal threshold value for each frame. The threshold value between 80 and 120, as seen in Fig. 6, was taken to determine which value has a green line fit to the interfacial water-air for each frame.

The candidate from the previous processing is shown in Fig. 7. Each frame has a different threshold value. The candidate frame will be compared with the ground truth image, with a red line representing the interface of air and water. The yellow line in the middle of the image is a guideline that divides the upper and lower images – the partition line. For the 1000th frame, the upper portion of the 110 is a good fit for the interface, while the lower portion benefits from the 120. However, for the 2000th frame, the higher section is better suited for the 100 rather than the 110, and the bottom section is better with the 110 rather than the 100. Finally, for frame 3000th, a value of 90 is the best in the upper section, and for the lower section, 100 is the best. The next step is to combine the upper section's optimum threshold values with the lower section's optimum value

C) Optimization process

Optimization improves the image by establishing the most favorable limits and threshold values. Optimization is achieved through the division of two pictures, wherein each segment is assigned a distinct threshold value. Enhancing the image and dividing the image area can be seen in Algorithm 2 and Algorithm 3.

Mathematical formulation of the image pre-processing algorithm:

1) Brightness Adjustment

For each pixel at position (i,j) in the input grayscale image, the enhanced image is computed as:

$$enhanced\_image(i,j) = gray\_image(i,j) + incr\_brightness \quad (2)$$

2) Thresholding

After adjusting the brightness, the image is thresholded to create a binary image. The binary image is computed as :

$$binary_{image(i,j)} = \begin{cases} 255 & if\ enhanced\_image(i,j) > threshold \\ 0 & otherwise \end{cases} \quad (3)$$

3) Morphological Closing

The binary image undergoes a morphological closing operation, which is a dilation followed by erosion using a structuring element K:

$$image_{morphology} = (binary\_image \oplus K) \ominus K \quad (4)$$

where:
$\oplus$ *denotes the dilation operation*:

$$dilated(i,j) = \max_{(m,n) \in K} enhanced\_image(i-m, j-n) \quad (5)$$

$\ominus$ *denotes the erosion operation:*

$$eroded(i,j) = \min_{(m,n) \in K} dilated(i+m, j+n) \quad (6)$$

Mathematical formulation of the Thresholding algorithm:

1) Load and convert the image to grayscale

In these equations:

(i,j) is the coordinates of the pixel in the image.

(m,n) is the coordinates relative to the center of the structuring element *K*

The structuring element *K* is typically a small matrix (e.g., 3×3) that defines the neighborhood over which the maximum (for dilation) or minimum (for erosion) is computed.

Input image loaded from *file_name* and *gray* be the grayscale version of the image:

$$gray = ConvertToGray(ReadImage(file\_name))$$

2) Determine image dimensions and split

W the width of the grayscale image gray:

$$W = CalculateWidthSize(gray) \quad (7)$$

Calculate the middle point:

$$middle = \frac{W}{2} \quad (8)$$

Algorithm 2: Image Pre-processing

Input: *gray_image,threshold*
Output: *enhanced_image,image_morphology*
Data: *incr_brighrness*
for *each row* **do**
  for *each column* **do**
    enhaced_image[row,column] ← *gray_image[row,column]* + *incr_brightness*
for *each row* **do**
  for *each column* **do**
    if *enhaced_image[row,column]>threshold* **then**
      enhaced_image[row,column]←255
    else
      enhaced_image[row,column]←0
kernel← $M_{3\times3}$
image_morphology[row,column]← ***closing****(enhanced_threshold, kernel)*

Algorithm 3: Thresholding

Input: *file_namne*
Output: *left_gray,right_gray,left_threshold*
Output: *right_threshold,left_threshold*
Output: *left_morphogy*
Data: *image,left_threshold*←*100*
right_threshold←*92*
/* Load the image */
image←ReadImage*(file_name)* /* Convert the image to gray */
gray←**ConvertToGray***(image)*
width←**CalculateWithSize***(gray)*
middle←*width/2*
area_left←*gray[:,0:middle]*
area_right←*gray[:,middle:width]*
left_gray,left_threshold,left_morphology←
PreprocessImage*(area_left,left_threshold)*
right_gray,right_threshold,right_morphology←
PreprocessImage*(area_right,right_threshold)*

Split the grayscale image into left and right parts:

Left part:

$$area\_left = gray[:, 0:middle] \quad (9)$$

$$area\_right = gray[:, middle:W] \quad (10)$$

Right part:

3) Preprocessing with thresholding and morphology

Apply preprocessing, including thresholding and morphological operations, to both parts:

Left part:

Thresholding:

$$left\_gray(i,j) = \begin{cases} 255 & if\ area\_left(i,j) > left\_threshold \\ 0 & otherwise \end{cases} \quad (11)$$

Morphological Operations

$$left\_morphology = MorphologicalOperations(left\_gray) \quad (12)$$

Right part:

Thresholding:

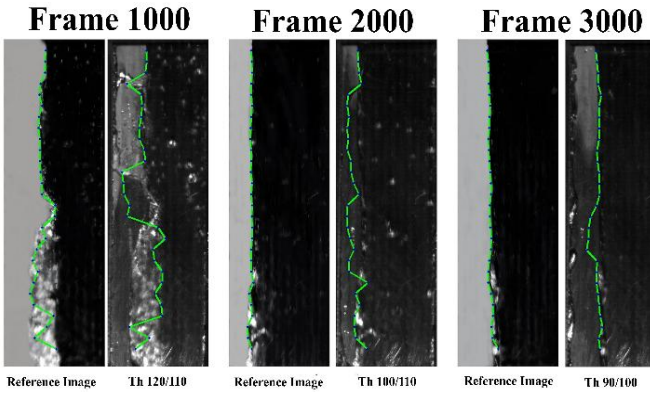

Figure. 8 Optimization using different threshold

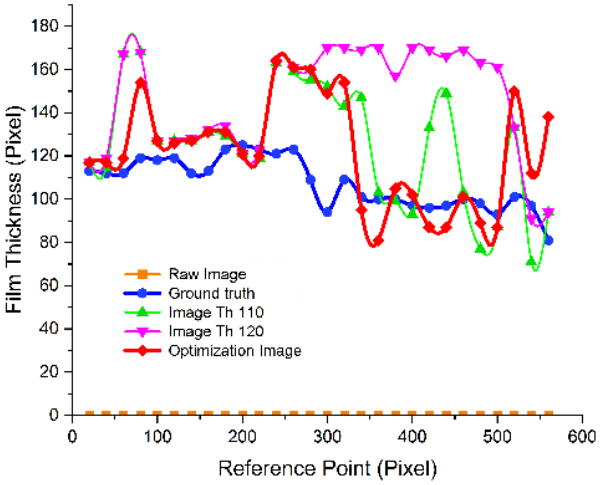

Figure. 9 Film thickness for various image processes in frame 1000th

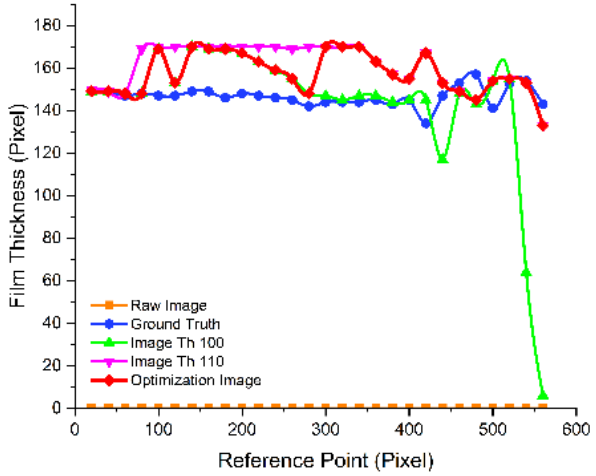

Figure.10 Film thickness for various image processes in frame 2000th

$$right\_gray(i,j) = \begin{cases} 255 & if\ area\_right(i,j) > right\_threshold \\ 0 & otherwise \end{cases} \quad (13)$$

where right threshold = 92

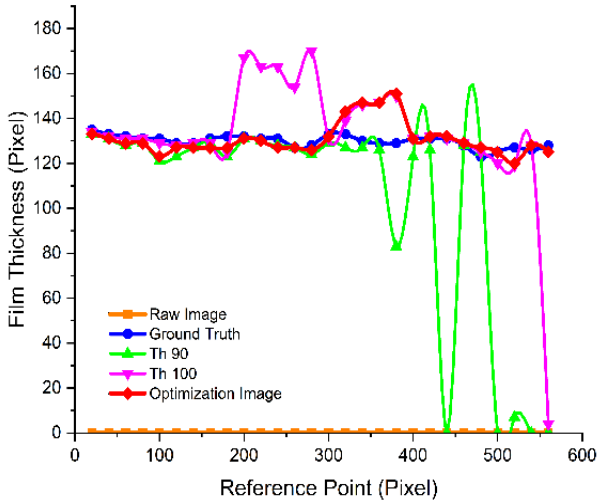

Figure. 11 Film thickness for various image processes in frame 3000th

Table 2. The Summary of The RMSE Result

Frame	Raw Image	Optimized image	Threshold			
			90	100	110	120
1000th	107,96	26,49	54,45	27,97	35,37	29,54
2000th	146,71	15,83	51,70	33,34	32,72	59,37
3000th	129,89	7,16	65,32	28,26	46,20	55,58

Morphological Operation :

$$right\_morphology = MorphologicalOperations(left\_gray) \quad (14)$$

This full mathematical representation provides a detailed view of the image processing steps performed in the thresholding algorithm, ensuring a clear understanding of how the image data is manipulated and processed.

By applying them, a combination of the optimal threshold values obtained from previous processing is carried out. The processing results obtain images for frames 1000th, 2000th, and 3000th. The threshold combination value is determined by choosing a threshold value that results in an image that closely resembles the reference image. For frame 1000th, a combination of threshold values of 120 was chosen for the upper area and 110 for the lower area, while for frames 2000th and 3000th, threshold values of 100 – 110 and 90 – 100 were chosen. Fig. 8 shows the results of using a combination of threshold values compared to the reference image.

From the film thickness data on frames 1000th, 2000th, and 3000th, comparisons were made between image optimization results with ground truth and images with thresholds 90, 100, 110, and 120. The comparison was conducted by graphically charting the thickness of the film layer and assessing the

degree of resemblance in the curves using human visual perception. It is shown in Figs. 9-11.

Based on the result—observations made on frame 1000th, as shown in Fig. 9, it was obtained that for reference points 0–300, the image results in optimization, and the image with the threshold 120 is close to the ground truth value. At reference points 300 – 560, images with threshold 110 and image optimization results are close to their ground truth curve. Image optimization with a combination of thresholds 120 and 110 has a better curve trend than images with thresholds 120 at reference points 60 and 80. Next, at reference points 300 – 560, image optimization follows the curve trends of images with thresholds 110. Generally, the image optimization results are better visually when approaching the ground truth curve.

From the results of the observations on frame 2000th, as seen in Fig. 10, the reference point 0-300, the image result optimization, and the image with threshold 100 are close to ground truth. The value of the thresholding 110 is far deviating from the ground truth at the range of reference points 80, 110, 220-280 mm. At the reference point 300–560, the image result threshold 100 is near ground truth, whereas the image optimization result is closer to ground truth at the reference point 460-560.

Image optimization with the combination of the thresholds 100 and 110 turns out to have the same trend as the thresholds 100 of the referenced point (20–290) and the reference points 280–560, following the image trend curve from the threshold 110. Generally speaking, optimization results are better visually in keeping with the ground truth curve.

From the observation results obtained on frame 3000th, as seen in Fig. 11, for reference point 0 - 300, image result optimization and image with threshold-

$$RMSE = \sqrt{\frac{\sum_{i=1}^{n}(Xobs_i - Xmodel_i)^2}{n}} \quad (15)$$

Where

$Xobs_i$	is	the observed value at the *i*-th data point,
$Xmodel_i$	is	the predicted or modeled value at the *i*-th data point, and
n	is	the total number of data points.

90 closes to the ground truth curve at the reference point 300–560, image results optimization and images with threshold 100 near the ground truth curve and image optimization with a combination of thresholds of 90 and 100 can approach the ground reality curve on frame 3000th.

To compare the raw image, processed image, and ground truth as an ideal image, use *Root Mean Square Error* (RMSE). The RMSE of a prediction model is defined as the square root of the mean (Eq.1), where $Xobs$ represents observed values and $Xmodel$ represents modeled values at a given time or location. The ground truth image's film thickness value represents the value of $Xobs$, and the optimization image's film thickness represents the value of $Xmodel$.

The proposed method rigorously quantifies the difference between ground truth and optimized images using RMSE, with lower values indicating enhanced accuracy and minimal deviation. As demonstrated in Table 2, RMSE values for frames 1000, 2000, and 3000 were significantly reduced to 26.49, 15.83, and 7.15, respectively, following optimization. Notably, the optimized image for frame 1000, using combined thresholds of 120 and 110, exhibited the lowest RMSE value, outperforming both the raw image and those processed with individual thresholds of 90, 100, 110, and 120. This trend continued in frames 2000 and 3000, where optimized images with threshold combinations of 100 and 110, and 90 and 100, respectively, demonstrated markedly lower RMSE values compared to single-threshold images. These results underscore the robustness of the optimization method in reducing deviation from the ground truth and significantly improving overall image accuracy.

Visual observations and RMSE comparisons consistently support these findings, demonstrating that the optimized image processing technique substantially enhances image quality and accurately determines film thickness. The method achieved RMSE reductions percentage up to 94.50% for frame 3000, with reductions of 75.45% and 89.21% for frames 1000 and 2000, respectively, compared to raw images.

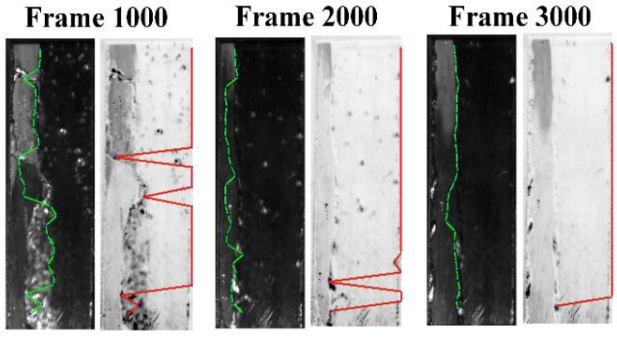

(a) (b) (a) (b) (a) (b)

Figure. 12 Comparation identification method: (a) Proposed method and (b) state-of-the art method

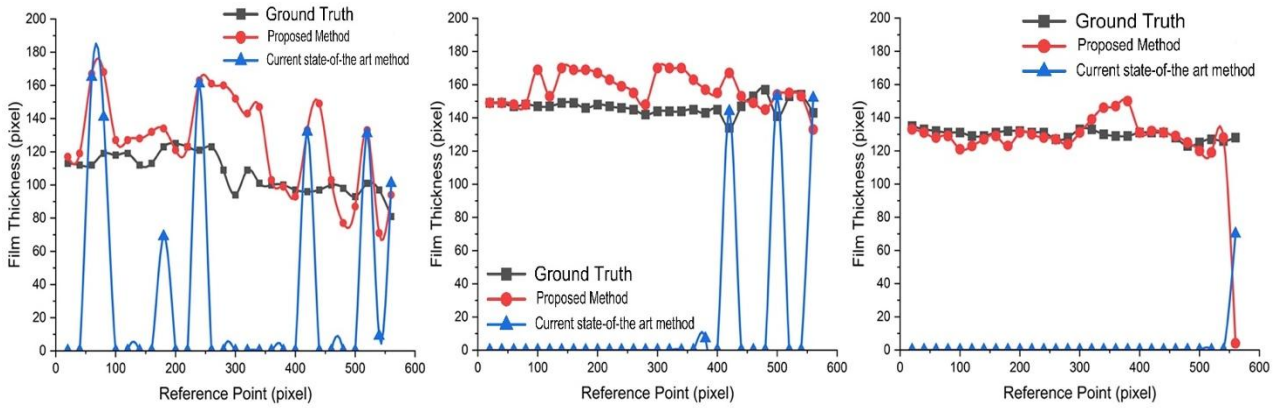

Figure. 13 Film thickness for ground truth, Proposed method and state-of-the art method frame: (a) 1000th, (b)2000th, and (c) 3000th

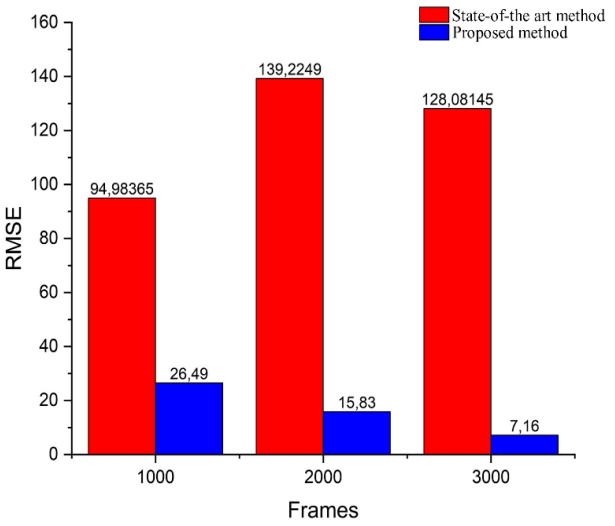

Figure. 14 RMSE Comparison: Proposed method vs state-of-the art method

The proposed method can enhance the quality of raw images and accurately determine film thickness, as seen by both visual analysis and computations utilizing the RMSE. A clear and direct comparison between the proposed method and state-of-the art method is shown in Fig. 12, as referenced in [27] and utilized in a recent study [39] is shown in Fig 12. In this comparison, the same raw image was processed using both approaches. Image (a) illustrates the output of the proposed methods, while Image (b) displays the results of the state of the state-of-the art method. The differences are striking: the green line in Image (a), generated by the proposed methods, precisely and reliably identifies the wave interface. Conversely, the red line in Image (b), produced by the state-of-the art method, demonstrates a noticeable inability to accurately detect the wave interface.

This stark contrast underscores the significantly superior performance of the proposed method in interface identification across all image samples. This superiority is further validated by the film thickness graphs and RMSE values. A closer fit of the curve to the reference curve at each reference point indicates greater accuracy. Additionally, a lower RMSE value signifies less deviation from the reference image, further confirming the proposed method's accuracy.

Fig. 13 illustrates the accuracy of the proposed method across different frames. In (a) frame 1000, (b) frame 2000, and (c) frame 3000, the red line, representing the proposed method, closely follows

the reference image (black line), whereas the blue line, representing the state-of-the art method, deviates significantly from the reference.

The results, as confirmed by the RMSE values, clearly demonstrate that the proposed method achieves superior precision across all frames compared to the state-of-the art method, as shown in Fig. 14. Since RMSE is a measure of error, lower RMSE values indicate better accuracy. By calculating the inverse of the RMSE, the improvement in accuracy can be expressed as a percentage increase when transitioning from the state-of-the art method to the proposed method.

The accuracy improvement is remarkable: for the first data point, accuracy increases by approximately 258.55%, for the second data point by 779.50% and for the third data point by an impressive 1688.85%. On average, the proposed method enhances accuracy by 908.97%, highlighting its substantial advantage over the state-of-the art method. It demonstrates an exceptional capability to manage image complexities and achieve more precise and robust interface identification. The findings from this study firmly establish the proposed method as a significant advancement, enhancing raw image quality and dramatically improving the accuracy of wave

identification in two-phase flows, thereby solidifying its superiority over existing techniques

6. Conclusion

This study presents a robust image processing method for wave identification in two-phase flows, particularly within narrow rectangular channels. The proposed method employs sequential multi-thresholding and image bisection techniques to enhance image segmentation and improve accuracy in identification wave interfaces and measuring liquid film thickness. Supported by morphological operations and brightness adjustments, the method effectively processes low-quality images, achieving RMSE reductions of 75.45%, 89.21%, and 94.50% for frames 1000, 2000, and 3000, respectively.

The Experimental results validate the robustness and effectiveness of the approach, demonstrating significant improvements in image quality and measurement accuracy. The method's adaptability to narrow-gap geometries and its robustness under suboptimal imaging conditions establish it as a reliable tool for real-time and industrial applications. The scalability and computational efficiency of the technique further ensure its suitability for safety-critical applications, such as nuclear reactor cooling systems during post-accident scenarios.

The theoretical foundation of this method is grounded in sequential multi-thresholding and image bisection for dynamic segmentation, supported by morphological operations for noise reduction and connectivity enhancement. Together, these techniques form a robust image processing pipeline, ensuring accuracy and scalability under diverse conditions.

The scientific contribution of this research lies in advancing non-intrusive wave identification techniques through innovative image processing methods. The proposed method addresses persistent challenges such as low-quality imaging, narrow-channel adaptability, and computational scalability, offering a transformative solution for industrial and real-time applications. Future work could explore extending this method to handle more complex flow environments, integrating it with machine learning for adaptive thresholding, and further enhancing its real-time performance.

This study establishes a strong foundation for improving two-phase flow analysis and contributes significantly to advancing the accuracy, reliability, and scalability of wave identification methods in critical engineering applications.

Conflicts of Interest

The authors declare no conflict of interest.

Author Contributions

Conceptualization, Nur Rahmad Yusuf and Suprapto; methodology, Nur Rahmad Yusuf, Suprapto, Jazi Eko and Deendarlianto; software, Nur Rahmad Yusuf; validation, Nur Rahmad Yusuf, Suprapto; formal analysis, Nur Rahmad Yusuf, Suprapto, Jazi Eko and Deendarlianto ; investigation, Nur Rahmad Yusuf; data curation, Nur Rahmad Yusuf, Suprapto, Jazi Eko and Deendarlianto; writing—original draft preparation, Nur Rahmad Yusuf; writing—review and editing, Suprapto, Jazi Eko and Deendarlianto; visualization, Nur Rahmad Yusuf; supervision, Suprapto, Jazi Eko and Deendarlianto.

References

[1] Becker and S. M., "The fukushima dai-ichi accident:report by the director general", *Vienna,Austria*, 2015, doi: 10.1097/HP.0b013e31829c351d.

[2] J. L. Rempe, L. A. Stickler, G. E. Korth, D. R. Diercks, L. A. Neimark, D. W. Akers, B. K. Schuetz, T. L. Shearer, S. A. Chdvez, G. L. Thinnes, R. J. Witt, M. L. Corradini, J. A. Kos, I. National, and U. S. N. R. Commission, "TMI-2 Vessel Investigation Project Integration Report", *IDAHO*, 1994.

[3] P. D. W. Bottomley, C. T. Walker, D. Papaioannou, S. Bremier, P. Pöml, J. P. Glatz, S. Van Winckel, P. Van Uffelen, D. Manara, and V. V. Rondinella, "Severe accident research at the Transuranium Institute Karlsruhe: A review of past experience and its application to future challenges", *Ann. Nucl. Energy*, Vol. 65, pp. 345-356, 2014, doi: 10.1016/j.anucene.2013.11.012.

[4] M. Juarsa, N. Putra, W. N. Septiadi, and A. R. Antariksawan, "Experimental study on the effect of gap size to CCFL and CHF in a vertical of narrow rectangular channel during quenching process", *Ann. Nucl. Energy*, Vol. 72, pp. 391-400, 2014, doi: 10.1016/j.anucene.2014.06.007.

[5] A. Setyawan, Indarto, and Deendarlianto, "The effect of the fluid properties on the wave velocity and wave frequency of gas-liquid annular two-phase flow in a horizontal pipe", *Exp. Therm. Fluid Sci.*, Vol. 71, pp. 25-41, 2016, doi: 10.1016/j.expthermflusci.2015.10.008.

[6] N. Andritsos, C. Tzotzi, and T. J. Hanratty, "INTERFACIAL SHEAR STRESS IN WAVY

STRATIFIED GAS-LIQUID TWO-PHASE FLOW", In: *Proc. of 5th Eur. Therm. Conf.*, pp. 0-7, 2008.

[7] H. C. Kang and M. H. Kim, "Measurement of three-dimensional wave form and interfacial area in an air-water stratified flow", *Nuclear Engineering and Design*, Vol. 136, No. 3. pp. 347-360, 1992, doi: 10.1016/0029-5493(92)90033-R.

[8] J. Shi and G. Kocamustafaogullari, "Interfacial measurements in horizontal stratified flow patterns", *Nuclear Engineering and Design*, Vol. 149, No. 1-3. pp. 81-96, 1994, doi: 10.1016/0029-5493(94)90276-3.

[9] A. Al-Sarkhi, C. Sarica, and K. Magrini, "Inclination effects on wave characteristics in annular gas-liquid flows", *AIChE Journal*, Vol. 58, No. 4. pp. 1018-1029, 2012, doi: 10.1002/aic.12653.

[10] W. Meng, "Low liquid loading gas-liquid two-phase flow in near-horizontal pipes", *UMI Company, Oklahoma*, 1999.

[11] K. Gawas, H. Karami, E. Pereyra, A. Al-Sarkhi, and C. Sarica, "Wave characteristics in gas-oil two phase flow and large pipe diameter", *Int. J. Multiph. Flow*, Vol. 63, pp. 93-104, 2014, doi: 10.1016/j.ijmultiphaseflow.2014.04.001.

[12] C. Tzotzi and N. Andritsos, "Interfacial shear stress in wavy stratified gas-liquid flow in horizontal pipes", *Int. J. Multiph. Flow*, Vol. 54, pp. 43-54, 2013, doi: 10.1016/j.ijmultiphaseflow.2013.03.003.

[13] G. A. Montoya, Deendarlianto, D. Lucas, T. Höhne, C. Vallée, T. H¨ohne, and C. Vall´ee, "Image-processing-based study of the interfacial behavior of the countercurrent gas-liquid two-phase flow in a hot leg of a PWR", *Sci. Technol. Nucl. Install.*, Vol. 2012, pp. 1-10, 2012, doi: doi:10.1155/2012/209542.

[14] H. Y. Kuntoro, A. Z. Hudaya, O. Dinaryanto, A. I. Majid, and Deendarlianto, "An improved algorithm of image processing technique for film thickness measurement in a horizontal stratified gas-liquid two-phase flow", In: *Proc. of AIP Conference Proceedings*, 2016, Vol. 1737, No. 1. doi: 10.1063/1.4949298.

[15] T. Q. kadhim, H. G. Daway, and A. M. Kadhim, "Enhancement of Lightness Image Based on DCP with Color Restoration and Lightness Mapping", *Int. J. Intell. Eng. Syst.*, Vol. 17, No. 1, pp. 689-697, 2024, doi: 10.22266/ijies2024.0229.58.

[16] C. E. F. do Amaral, R. F. Alves, M. J. Da Silva, L. V. R. Arruda, L. Dorini, R. E. M. Morales, and D. R. Pipa, "Image processing techniques for high-speed videometry in horizontal two-phase slug flows", *Flow Meas. Instrum.*, Vol. 33, pp. 257-264, 2013, doi: 10.1016/j.flowmeasinst.2013.07.006.

[17] A. Widyatama, O. Dinaryanto, Indarto, and Deendarlianto, "The development of image processing technique to study the interfacial behavior of air-water slug two-phase flow in horizontal pipes", *Flow Meas. Instrum.*, Vol. 59, No. 2017, pp. 168-180, 2018, doi: 10.1016/j.flowmeasinst.2017.12.015.

[18] I. Mantilla, L. Gomez, R. Mohan, O. Shoham, G. Kouba, R. Roberts, L. Gomez, R. Mohan, and O. Shoham, "Experimental investigation of liquid entrainment in gas in horizontal pipes", In: *Proc. of the ASME 2009 Fluids Engineering Division Summer Meeting*, Vol. 1, pp. 1-27, 2009, doi: 10.1115/FEDSM2009-78420.

[19] C. E. F. Do Amaral, R. F. Alves, M. J. Da Silva, L. V. R. Arruda, L. B. Dorini, and R. E. M. Morales, "Bubble identification based on high speed videometry data: Algorithm and validation", *Progress in Pattern Recognition, Image Analysis, Computer Vision, and Applications*, Vol. 7441 LNCS, pp. 870-876, 2012, doi: 10.1007/978-3-642-33275-3_107.

[20] A. H. Astyanto, I. Indarto, and D. Deendarlianto, "A Brief on Optical-based Investigation towards The Interfacial Behaviors during High Viscous Liquid / Gas Countercurrent Two-Phase Flow in a Complex Conduit Representing 1/30 Down-Scaled of PWR Hot Leg Geometry", *Int. J. Appl. Sci. Smart Technol.*, Vol. 5, No. 1, pp. 101-112, 2023, doi: 10.24071/ijasst.v5i1.6302.

[21] S. L. G. haralick Robert M, *computer and robot vision*, 1st ed. Seattle, Washington: Addison-Wesley Publishing Company, 1992.

[22] NOBUYUKI OTSU, "A Threshold Selection Method from Gray-Level Histograms", *IEEE Trans. Syst. Man. Cybern.*, Vol. C, No. 1, pp. 62-66, 1979.

[23] S. Wijayanta, Indarto, Deendarlianto, I. G. N. B. Catrawedarma, and A. Z. Hudaya, "Statistical characterization of the interfacial behavior of the sub-regimes in gas-liquid stratified two-phase flow in a horizontal pipe", *Flow Meas. Instrum.*, Vol. 83, No. 2, p. 102107, 2022, doi: 10.1016/j.flowmeasinst.2021.102107.

[24] A. N. A. Nugroho, Deendarlianto, Indarto, and Achilleus Hermawan Astyanto, "Stochastic and wavelet analysis towards liquid film thickness fluctuations during countercurrent flow limitation on a complex geometry by using image processing", *AIP Conference Proceedings*, Vol. 2836, No. 1, pp. 1-10, 2024,

doi: 10.1063/5.0207224.
[25] R. C. Gonzalez and R. E. Woods, *Digital Image Processing*, 4th ed. Essex-England: Pearson Education Limited, 2018.
[26] Deendarlianto, A. Z. Hudaya, Indarto, and K. D. Ozzilenda Soegiharto, "Wetted wall fraction of gas-liquid stratified co-current two-phase flow in a horizontal pipe with low liquid loading", *J. Nat. Gas Sci. Eng.*, Vol. 70, p. 102967, 2019, doi: 10.1016/j.jngse.2019.102967.
[27] S. Wijayanta, A. Prasetyo, A. Zidni, Deendarlianto, and Indarto, "The effect of the liquid physical properties on the wave frequency and wave velocity of co-current gas-liquid stratified two-phase flow in a horizontal pipe", *Int. J. Multiph. Flow*, Vol. 158, No. 2, p. 104300, 2023, doi: 10.1016/j.ijmultiphaseflow.2022.104300.
[28] N. R. Yusuf, S. Kamal, M. Juarsa, R. Ainur, J. P. W. I. H, P. Kalor, P. Pada, and C. Sempit, "Analisis counter current flow limitation selama proses perpindahan kalor pendidihan pada celah sempit rektangular", *prosiding seminar keselamatan nuklir*, 2011.
[29] M. J. Nur Rahmad Yusuf, Samsul Kamal, "STUDI COUNTER CURRENT FLOW LIMITATION SELAMA PROSES PERPINDAHAN KALOR PENDIDIHAN PADA CELAH SEMPIT REKTANGULAR", *gajah mada university*, 2012.
[30] M. Juarsa, N. Putra, R. A. Koestoer, and A. R. Antariksawan, "The effect of gap size to ccfl in rectangular channel for double heated chase", In: *Proc. of Seminar Nasional Tahunan Teknik Mesin XI (SNTTM XI) & Thermofluid IV*, No. Snttm Xi, pp. 747-752, 2012.
[31] R. K. S.S. Bedi, "Various Image Enhancement Techniques- A Critical Review", *Int. J. Adv. Res. Comput. Commun. Eng.*, Vol. 2, No. 3, pp. 1605-1609, 2013.
[32] K. Seshadrinathan, T. N. Pappas, R. J. Safranek, J. Chen, Z. Wang, H. R. Sheikh, and A. C. Bovik, *Image Quality Assessment*, 1st ed., No. December. Elsevier, 2009, doi: 10.1016/B978-0-12-374457-9.00021-4.
[33] Y. Qi, Z. Yang, W. Sun, M. Lou, J. Lian, W. Zhao, X. Deng, and Y. Ma, "A Comprehensive Overview of Image Enhancement Techniques", *Arch. Comput. Methods Eng.*, Vol. 29, No. 1, pp. 583-607, 2022, doi: 10.1007/s11831-021-09587-6.
[34] A. Z. Hudaya, A. Widyatama, O. Dinaryanto, W. E. Juwana, Indarto, and Deendarlianto, "The liquid wave characteristics during the transportation of air-water stratified co-current two-phase flow in a horizontal pipe", *Exp. Therm. Fluid Sci.*, Vol. 103, No. January, pp. 304-317, 2019, doi: 10.1016/j.expthermflusci.2019.01.021.
[35] J. Subash and J. Majumdar, "Comparison of Image Enhancement Algorithms for Improving the Visual Quality in Computer Vision Application", *Int. J. Adv. Comput. Sci. Appl.*, Vol. 13, No. 7, pp. 638-654, 2022, doi: 10.14569/IJACSA.2022.0130775.
[36] B. Bataineh, "Brightness and Contrast Enhancement Method for Color Images via Pairing Adaptive Gamma Correction and Histogram Equalization", *Int. J. Adv. Comput. Sci. Appl.*, Vol. 14, No. 3, pp. 124-134, 2023, doi: 10.14569/IJACSA.2023.0140314.
[37] Z. Wang, A. C. Bovik, H. R. Sheikh, and E. P. Simoncelli, "Image quality assessment: From error visibility to structural similarity", *IEEE Trans. Image Process.*, Vol. 13, No. 4, pp. 600-612, 2004, doi: 10.1109/TIP.2003.819861.
[38] W. H. Zhu, W. Sun, X. K. Min, G. T. Zhai, and X. K. Yang, "Structured Computational Modeling of Human Visual System for No-reference Image Quality Assessment", *Int. J. Autom. Comput.*, Vol. 18, No. 2, pp. 204-218, 2021, doi: 10.1007/s11633-020-1270-z.
[39] S. Wijayanta, Indarto, Deendarlianto, and C. Y. Sianipar, "The effect of the liquid viscosity on the liquid film thickness and wave frequency of the gas-liquid stratified co-current flow in horizontal pipes", *AIP Conference Proceedings*, Vol. 2836, No. 1, pp. 090005-1, 2024, doi: 10.1063/5.0188647.